

Simulation of terahertz plasmons in graphene with grating-gate structures

Akira Satou, Victor Ryzhii, and Taiichi Otsuji
 Research Institute of Electrical Communication
 Tohoku University, Sendai 980-8577, Japan
 Email: a-satou@riec.tohoku.ac.jp

Fedir T. Vasko* and Vladimir V. Mitin
 Department of Electrical Engineering
 University at Buffalo, Buffalo, NY 14260-1920, USA

Abstract—Frequency dispersion and damping mechanisms of two-dimensional plasmons in graphene in the terahertz (THz) range are studied by a numerical simulation based on the Boltzmann equation. The fundamental plasmon mode in a single-grating-gate structure is studied, and the coupling effect of plasmons in the gated and ungated regions are revealed. It is shown that the plasmon frequency as well as its gate-voltage tunability depend strongly on the coupling. It is also demonstrated that damping rates due to the acoustic-phonon scattering at room temperature and short- and finite-range disorder scattering can be on the order of 10^{11} s^{-1} , depending on the level of disorders.

I. INTRODUCTION

Graphene, a two-dimensional material made of carbon atoms, has been extensively researched due to its exceptional electronic and optical properties. Especially, it is very promising as a channel material of THz plasmonic devices which can surpass those based standard compound semiconductor heterostructures investigated for decades [1], [2].

One of the most important advantages of plasmons in graphene over those in heterostructure two-dimensional electron gases is a weaker damping rate close to 10^{11} s^{-1} at room temperature in disorder-free graphene limited only by the acoustic-phonon scattering. Such a weak damping rate enables the realization of resonant THz detection and also of THz emission through the occurrence of plasma instabilities, both at room temperature. In addition, interband population inversion in graphene in the THz range was predicted [3] and has been investigated for the utilization not only to THz lasers in the usual sense but also to THz active plasmonic devices [4], [5].

Previously, we have obtained the analytical expression of the frequency dispersion of plasmons in gated graphene based on the Boltzmann equation [6] and the hydrodynamic equations [7], and we have revealed that the plasma frequency can be in the THz range and can be widely tunable by the gate voltage. The damping due to the acoustic-phonon scattering and electron-hole friction has also been discussed [7]. In this paper, we develop a numerical model for the simulation of plasmons in more complex graphene structures, based on the Boltzmann equation for electron and hole transport coupled with the self-consistent Poisson equation. We consider a single-grating-gate structure with periodic boundaries and investigate the voltage tunability of the plasma frequency. We also study

the damping due to the acoustic-phonon scattering and due to the short- and finite-range disorder scattering.

II. NUMERICAL MODEL

Here, we consider a single-grating-gate structure which consists of a graphene channel with period length L , insulating substrate, dielectric layer with thickness W_g , gate with length L_g , and passivation layer above the gate (Fig. 1), with periodic boundary conditions. We use the quasi-classical Boltzmann equation to describe the electron and hole transport:

$$\frac{\partial f_r}{\partial t} + v_F \frac{p_x}{|\mathbf{p}|} \frac{\partial f_r}{\partial x} + s_r e E_x \frac{\partial f_r}{\partial p_x} = \sum_i J_i(f_r|\mathbf{p}), \quad (1)$$

where $v = 10^6 \text{ m/s}$ is the carrier velocity in graphene, $r = e$ and $r = h$ for electrons and holes together with $s_e = -1$ and $s_h = +1$, respectively, E_x is the self-consistent electric field in graphene, and $\mathbf{p} = (p_x, p_y)$ is the momentum. Here, we take into account collision integrals for acoustic-phonon scattering, J_{LA} , short-range disorder (point-defect) scattering, J_{DS} , and finite-range disorder (inhomogeneity) scattering, J_{DF} , where

$$J_i(f_r|\mathbf{p}) = \frac{1}{(2\pi\hbar)^2} \int d\mathbf{p}' W_i(\mathbf{p}' - \mathbf{p}) [f_r(\mathbf{p}') - f_r(\mathbf{p})] \quad (2)$$

and the explicit expressions of the transition probabilities W_i can be found in Ref. 8 for the acoustic-phonon scattering and in Ref. 9 for the others. In this paper, we restrict ourselves to the situation where the electron concentration is much larger than the hole concentration, so that coupled modes of electron and hole plasmas and their damping caused by the electron-hole friction predicted in Ref. 7 can be neglected. Equation (1)

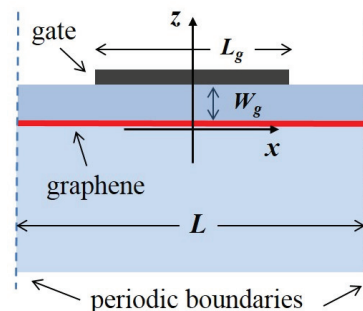


Fig. 1. Schematic view of the single-grating-gate structure.

*Present address: QK Applications, San Francisco, CA 94033, USA

is accompanied with the self-consistent Poisson equation

$$\nabla \cdot (\epsilon \nabla \varphi) = 4\pi e(\Sigma_e - \Sigma_h - \Sigma_d)\delta(z) \quad (3)$$

where φ is the electric potential, ϵ is the dielectric constant, $\Sigma_r = \int dp f_r / \pi^2 \hbar^2$ is the carrier concentration, and Σ_d is the doping concentration. The doping can be by the unintentional doping from the substrate and contacts and/or by the controlled remote doping from the dielectric layer. For simplicity we set $\epsilon = 4$. The boundary conditions for Eqs. (1) and (3) are periodic, i.e., $f_r|_{x=-L/2} = f_r|_{x=L/2}$ and $\varphi|_{x=-L/2} = \varphi|_{x=L/2}$. In addition, natural boundary conditions are set for the potential at $|z| \rightarrow \infty$. We adapt the so-called weighted essentially nonoscillatory finite-difference scheme [10] for solving Eq. (1). Equation (3) is solved using a software library libMesh [11], which is based on the finite-element method.

The simulation is divided into two parts. First, we find a self-consistent steady-state distribution function accounting for the gate voltage and the doping by conducting a transient simulation based on Eqs. (1) and (3) until the steady state is reached. Second, we add to the steady-state concentration a small artificial perturbation with sinusoidal variation in position (more precisely, $\delta\Sigma \propto \cos(2\pi x/L)$), simulate the plasma oscillation both in time and space, and extract the frequency and damping rate from the oscillation of the concentration. For the distinct analysis of the dispersion relation and the damping of plasmons, we shall study the former in the gated structure without any collision integrals and, hence, with no damping, while we shall study the latter in the ungated structure.

III. FREQUENCY OF PLASMONS IN SINGLE-GRATING-GATE STRUCTURE

Here, we study the dependence of plasmon frequencies on the gate voltage and gate length. We consider the single-grating-gate structure with the period length $L = 4 \mu\text{m}$, gate-to-channel thickness $W_g = 50 \text{ nm}$, and electron doping concentration $\Sigma_e = 5 \times 10^{11} \text{ cm}^{-2}$, and we vary the gate voltage $V_g = 0 - 8 \text{ V}$ and gate length $L_g = 800 - 3200 \text{ nm}$. The relatively high doping concentration here ensures that the electron-hole friction can be neglected. Profiles of the steady-state electron concentrations with different gate voltages and gate lengths are shown in Fig. 2. It can be seen that the electron concentration under the gate increases almost linearly to the voltage, while the concentration in the ungated region slightly increases due to the gate fringing effect. Since an initial sinusoidal perturbation set at the beginning of the simulation does not correspond to the fundamental mode of this complex structure, it yields the superposition of higher harmonics. We can extract the fundamental mode from it by performing the time-domain Fourier transform.

Figures 3 and 4 show the gate-voltage dependence of frequencies of the fundamental symmetric modes with different gate lengths and their mode profiles, respectively. It is clearly illustrated from Fig. 3 that the fundamental plasmon frequency of the structure is in the THz range, and that it can be tuned by the gate voltage. The frequency tunability becomes narrower with the shorter gate length. Also, there is a nontrivial feature of the dependence on the gate length when the gate voltage is fixed; there is a maximum frequency at a certain value of the gate length. These features can be explained qualitatively by the coupling of gated and ungated plasmons.

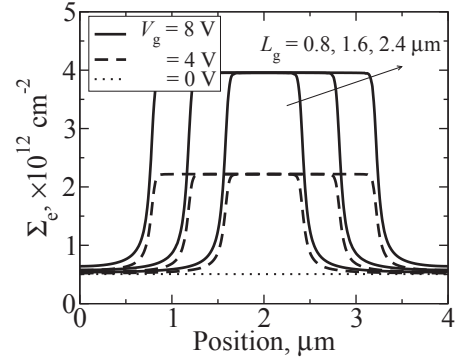


Fig. 2. Profiles of steady-state electron concentrations with different gate voltages V_g and different gate lengths L_g .

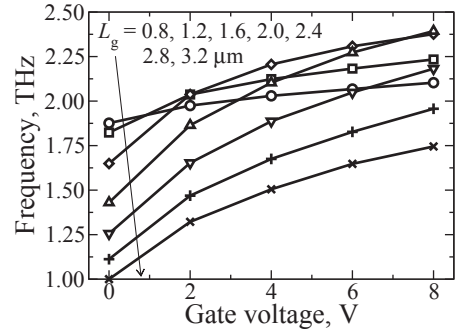


Fig. 3. Gate-voltage dependence of frequencies of the fundamental symmetric modes with different gate lengths L_g .

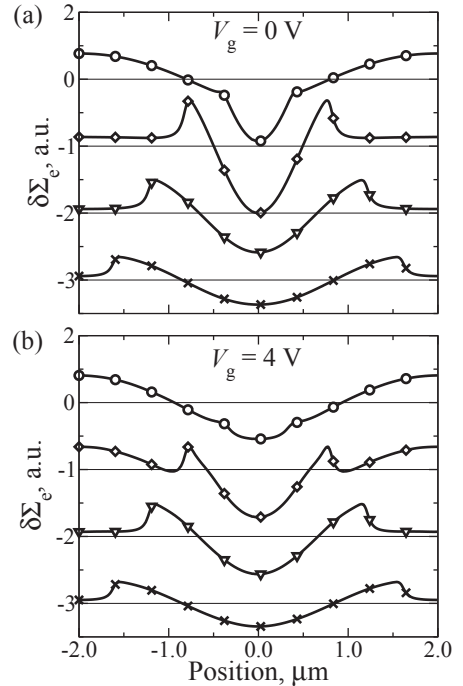


Fig. 4. Profiles of the fundamental symmetric modes with gate voltage (a) $V_g = 0 \text{ V}$ and (b) $V_g = 4 \text{ V}$, and with different gate lengths L_g (curves with circles, diamonds, triangles, and crosses for $L_g = 0.8, 1.6, 2.4,$ and $3.2 \mu\text{m}$, respectively). Each curve is shifted vertically by -1 , and thin solid lines correspond to $\delta\Sigma_e = 0$ for each curve.

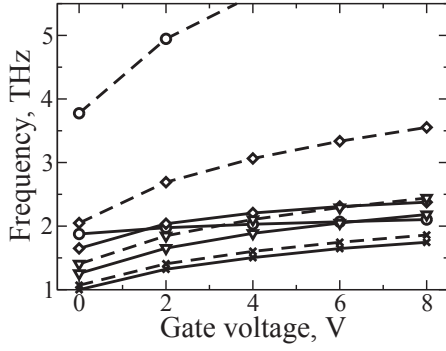


Fig. 5. Comparison of the gate-voltage dependence of frequencies for the single-grating-gate (solid curves) and fully-gated structures (dashed curves), with different gate lengths L_g (curves with circles, diamonds, triangles, and crosses for $L_g = 0.8, 1.6, 2.4,$ and $3.2 \mu\text{m}$, respectively).

Individually, frequencies of gated and ungated plasmons are proportional to k and \sqrt{k} , respectively, where k is the wavenumber [6], meaning that their frequencies become higher with the shorter length of the channel. Moreover, the frequency of ungated plasmon is higher than that of gated plasmon due to the gate screening effect, when the concentration and wavenumber are identical. Considering these, the gate length dependence can be explained as follows. First, for $V_g = 0$ V, the frequency monotonically increases as the gate length becomes shorter in Fig. 3. With $L_g = 3.2 \mu\text{m}$ (i.e., with the length of the ungated region $0.8 \mu\text{m}$) the frequency of the ungated plasmon is too high to be fully excited, so that the dominant oscillation takes place in the gated region, as illustrated in Fig. 4(a). This means the coupling of the gated plasmon to the ungated plasmon in this case is very weak. With the shorter gate length, the coupling becomes stronger, and the amplitude of the oscillation in the ungated region increases. At the same time, striking the gate length results in the frequency increase. The situation changes when the concentration is increased by the gate voltage, say, by $V_g = 4$ V; there is a maximum of the frequency with $L_g = 1.6 \mu\text{m}$. The coupling becomes strongest with this gate length, and both gated and ungated plasmons are excited (see Fig. 4(b)). With $L_g > 1.6 \mu\text{m}$ or $L_g < 1.6 \mu\text{m}$, either gated or ungated plasmon is dominantly excited, respectively. This indicates that the frequency in this structure takes maximum at the crossover point of the coupling of gated and ungated plasmons.

The frequency tunability depends strongly on the coupling as well. It is directly related to how dominant the gated plasmon is. With a long gate length (e.g., $L_g = 3.2 \mu\text{m}$) the gated plasmon is dominantly excited, so that the frequency tunability is effective and is almost comparable to that of a fully-gated structure, where the entire channel is covered by a gate (see Fig. 5). A small decrease in the frequency compared with the fully-gated structure is due to the weak but nonnegligible coupling to the ungated plasmon. On the other hand, with a short gate length (e.g., $L_g = 0.8 \mu\text{m}$) the coupling is strong, and the frequency is primarily determined by the ungated plasmon. This results in a poor frequency tunability as well as a huge decrease in the frequency compared with the fully-gated structure, as shown in Fig. 5.

These results indicate a great impact of the coupling of gated and ungated plasmons on the device design, especially,

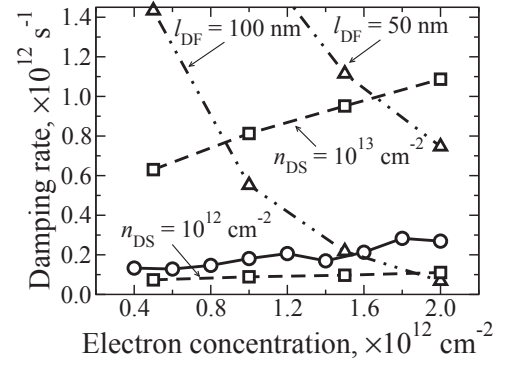


Fig. 6. Dependences of the damping rates due to the acoustic-phonon scattering at room temperature (a solid curve with circles), to the short-range disorder scattering (dashed curves with squares) with different defect concentrations n_{DS} , and to the finite-range disorder scattering (dashed-dotted curves with triangles) with different correlation length l_{DF} .

on the determination of the operating frequency as well as its tunability by the gate voltage.

IV. DAMPING BY CARRIER SCATTERING

Next, we discuss about the damping of plasmons by carrier scattering with acoustic phonons and short- and finite-range disorders. Here, we considered an ungated periodic structure with the uniform doping concentration Σ_d . The presence of the gate does not affect the acoustic-phonon scattering, whereas it may affect the finite-range disorder scattering because the screening of the interaction potential by carriers is suppressed [12] and, specifically, the damping rate might increase. However, the latter effect is expected to be not significant in case of structures with $W_g \geq 50$ nm and with the correlation length of the finite-range disorder $l_{DF} \leq 100$ nm which we shall focus on. Furthermore, we included each scattering mechanism separately to study their characteristics. The damping rate was extracted by taking the average of ratios of adjacent maxima and minima of the concentration oscillation which decays in time.

Figure 6 shows the dependences of the damping rates due to the acoustic-phonon scattering at room temperature and due to the short- and finite-range disorder scattering on the electron concentration. The dependences of the damping rates on the concentration come from that on the Fermi level and therefore from the energy-dependent scattering rate. As shown in Fig. 6, the damping rate of plasmons in disorder-free graphene, which is limited only by the acoustic-phonon scattering, can be down to $1.3 \times 10^{11} \text{ s}^{-1}$ at room temperature, demonstrating the feasibility of graphene-based plasmonic devices. The dependence agrees well with the analytical expression of the damping rate, $1/2\tau_{ACP}$, where τ_{ACP} is the acoustic-phonon-limited momentum relaxation time taken from Ref. 8.

As is evident from the expression of the transition probability in Ref. 9, the damping rate due to the short-range disorder scattering is proportional to n_{DS} . Figure 6 shows that the defect concentration on the order of 10^{12} cm^{-2} is permissible for graphene-based plasmonic devices. Contrary to the other two mechanisms, the damping rate due to the finite-range disorder dramatically decreases as the concentration increases above 10^{12} cm^{-2} ; even the damping rate can be below 10^{11}

s^{-1} with $2 \times 10^{12} \text{ cm}^{-2}$ and $l_{DF} = 100 \text{ nm}$. This is because electrons with larger wavenumber k feel the inhomogeneity less if $kl_{DF} \gg 1$. This dependence results in the existence of a minimum of the total scattering rate at some concentration, which varies depending on the level of disorders. The damping rate also decreases as the correlation length l_{DF} increases. Figure 6 suggests that the length should be longer than the order of 100 nm to achieve the damping rate comparable to or less than those for acoustic-phonon and short-range disorder scattering. The correlation length of this order can be achieved with samples having high quality comparable to suspended graphene.

V. CONCLUSION

We developed a numerical model for simulation of plasmons in complex gated graphene structures, based on the Boltzmann equation for electron and hole transport coupled with the self-consistent Poisson equation. Using the developed model, the fundamental plasmon mode in the single-grating-gate structures was studied. It was revealed that the frequency and its gate-voltage tunability depend strongly on the lengths of gated and ungated regions in the channel through the dependence of the coupling of plasmons in these region, indicating its great impact on the device design. The damping caused by carrier scattering was also studied. It was demonstrated that the damping rates due to the acoustic-phonon scattering at room temperature and due to the short-range (point-defect) and finite-range (inhomogeneity) disorder scattering can be on the order of 10^{11} s^{-1} , depending on the level of disorders and on the electron concentration.

ACKNOWLEDGMENT

This work was supported by JSPS Grant-in-Aid for Specially Promoted Research (#23000008) and by JSPS Grant-in-Aid for Young Scientists (B) (#23760300). The computation was mainly carried out using the computer facilities at Research Institute for Information Technology, Kyushu University, and at Information Technology Center, the University of Tokyo.

REFERENCES

- [1] M. Dyakonov and M. Shur, "Shallow water analogy for a ballistic field effect transistor: new mechanism of plasma wave generation by dc current," *Phys. Rev. Lett.*, vol. 71, pp. 2465–2468, 1993.
- [2] —, "Detection, mixing, and frequency multiplication of terahertz radiation by two-dimensional electronic fluid," *IEEE Trans. Electron Devices*, vol. 43, no. 3, pp. 380–387, 1996.
- [3] V. Ryzhii, M. Ryzhii, and T. Otsuji, "Negative dynamic conductivity of graphene with optical pumping," *J. Appl. Phys.*, vol. 101, p. 083114, 2007.
- [4] A. A. Dubinov, V. Y. Aleshkin, V. Mitin, T. Otsuji, and V. Ryzhii, "Terahertz surface plasmons in optically pumped graphene structures," *J. Phys.: Condens. Matter*, vol. 23, p. 145302, 2011.
- [5] V. Popov, O. Polischuk, A. Davoyan, V. Ryzhii, T. Otsuji, and M. Shur, "Plasmonic terahertz lasing in an array of graphene nanocavities," *Phys. Rev. B*, vol. 86, p. 195437, 2012.
- [6] V. Ryzhii, A. Satou, and T. Otsuji, "Plasma waves in two-dimensional electron-hole system in gated graphene heterostructures," *J. Appl. Phys.*, vol. 101, p. 024509, 2007.
- [7] D. Svintsov, V. Vyurkov, S. Yurchenko, T. Otsuji, and V. Ryzhii, "Hydrodynamic model for electron-hole plasma in graphene," *J. Appl. Phys.*, vol. 111, p. 083715, 2012.
- [8] E. Hwang and S. Das Sarma, "Acoustic phonon scattering limited carrier mobility in two-dimensional extrinsic graphene," *Phys. Rev. B*, vol. 77, p. 115449, 2008.
- [9] F. Vasko and V. Ryzhii, "Voltage and temperature dependencies of conductivity in gated graphene," *Phys. Rev. B*, vol. 76, p. 233404, 2007.
- [10] J. A. Carrillo, I. M. Gamba, A. Majorana, and C.-W. Shu, "A WENO-solver for the transients of Boltzmann-Poisson system for semiconductor devices: performance and comparisons with Monte Carlo methods," *J. Comp. Phys.*, vol. 184, pp. 498–525, 2003.
- [11] B. S. Kirk, J. W. Peterson, R. H. Stogner, and G. F. Carey, "libMesh: a C++ library for parallel adaptive mesh refinement/coarsening simulations," *Eng. Comp.*, vol. 22, pp. 237–254, 2006.
- [12] F. Vasko, V. Mitin, V. Ryzhii, and T. Otsuji, "Interplay of intra- and interband absorption in a disordered graphene," *Phys. Rev. B*, vol. 86, p. 235424, 2012.